minerals

MDPI

Article

Material Characterization of Mayapán's Effigy Censers' Sherds

Miguel Pérez [1,2], Oscar G. de Lucio [2,*], Alejandro Mitrani [2], Carlos Peraza Lope [3], Wilberth Cruz Alvarado [3] and Soledad Ortiz Ruiz [4]

[1] Investigador Posdoctoral CONACyT, Instituto de Física, Universidad Nacional Autónoma de México, Apartado Postal 20-364, Mexico City 01000, Mexico; mperez@fisica.unam.mx
[2] Laboratorio Nacional de Ciencias Para la Investigación y la Conservación del Patrimonio Cultural, Instituto de Física, Universidad Nacional Autónoma de México, Apartado Postal 20-364, Mexico City 01000, Mexico; mitrani@fisica.unam.mx
[3] Centro INAH Yucatan, Km. 65 Carretera Progreso, Mérida 97000, Mexico
[4] Investigador Posdoctoral-CONACyT, Instituto de Geofísica, Unidad Michoacán, Universidad Nacional Autónoma de México, Campus Morelia, Antigua Carretera a Pátzcuaro No. 8701, Col. Ex-Hacienda de San José de La Huerta, Morelia 58190, Mexico; sole.ortiz.ruiz@gmail.com
* Correspondence: olucio@ciencias.unam.mx

Abstract: Ceramic production from ancient Mesoamerican civilizations is related with cultural and technological evolution processes. Studying ritual objects also provides information on ancient traditions and allows researchers to determine the importance of certain materials employed in its manufacture. In this work, a set of 72 of Mayapán's effigy censers' sherds was analyzed in situ by using a combination of non-invasive, non-destructive spectroscopic and imaging techniques for material characterization; colorimetry established an initial classification of the pigments present in the objects, XRF provided elemental information, FORS allowed us to describe the molecular characteristics, and hyperspectral imaging established compositional contrasts or similitudes between large regions of the different objects. Pigments were characterized, allowing us to describe the materials used in the decorations of such ritual objects. The pottery matrix was also characterized, leading to a detailed description of the clays and mixtures of minerals employed in the construction of the effigy censers.

Keywords: mineral pigments; ritual pottery; hyperspectral imaging; XRF; FORS; Heritage Sciences

Citation: Pérez, M.; de Lucio, O.G.; Mitrani, A.; Peraza Lope, C.; Cruz Alvarado, W.; Ortiz Ruiz, S. Material Characterization of Mayapán's Effigy Censers' Sherds. *Minerals* **2023**, *13*, 974. https://doi.org/10.3390/min13070974

Academic Editors: Luminita Ghervase, Monica Dinu and Ioana Maria Cortea

Received: 25 May 2023
Revised: 17 July 2023
Accepted: 19 July 2023
Published: 22 July 2023

1. Introduction

Mayapán is located 40 km southeast of Mérida in the Yucatán peninsula in Mexico. This pre-Hispanic settlement is currently considered to be the last Maya capital of the Postclassic period (1100–1450 CE). Mayapán's importance resides not only in its territorial expansion, but also in the number and volume of its structures and in the magnificent archaeological material finds, such as diverse types of ceramics, lithic artifacts, shell and jade objects, and colorful mural paintings.

An outstanding feature of Mayapán is the presence of the surrounding wall, which has been associated directly with a defensive function. Within the boundaries of the wall, there are a significant number of structures (some still unexplored). The main buildings in Mayapán are present in a compact arrangement surrounding Kukulcán Castle, forming the Principal Group. There are also some isolated ceremonial structures scattered over the rest of the city. Pollock [1] estimated the population of Mayapán at about 10,000 people, living in over 2000 habitational structures, using about the same number of domestic buildings and over 100 ceremonial structures, thus having about 4000 structures in the city [2]. A prospective study developed between 2001–2004 by Bradley Russell [3] estimated that a population of about 17,000 people lived outside the wall, covering an area of around 10 square kilometers.

Different sources (Chilam Balam de Chumayel [4], de Tizimín [5] (1982: 10) de Maní (Códice Pérez 1949: 165) [6], and Fray Diego de Landa (1986: 17, 20) [7]) agree on the date of the destruction of Mayapán, dating it in *katún 8 Ahau*, which is situated somewhere between 1441–1460 A.D.

Effigy censers are recognized as the most important type of ceramics found in Mayapán. In this work, two kinds of censers were studied: The ***Chen Mul*** modeled type, defined by Smith in 1971 [8], belongs to the Unslipped Panaba Group of Mayapán Unslipped Ware of the Tases ceramic complex (A.D. 1250/1300–1450). The ***Hoal*** modeled type, which is also mentioned by Smith [8] as characteristic of the Hocaba phase (A.D. 1100–1250/1300), seems to have existed before the development of the ***Chen Mul*** type in the Hocaba-Tases transition (A.D. 1250) [8,9]. It is estimated that this kind of sherd represents about a quarter of the total ceramic deposits found in the city [9,10]. As described by Milbrath [9–11], these types of effigy censers present different figures attached to a cylindrical vase with a flaring pedestal base and a rim. A concave floor with openings is believed to have provided a draft for burning *copal*, as this resin is usually found on the floor along with fire blackening marks. The elbows of the figures are bent, and they present their offerings with their hands raised. Censers have been found painted in multiple colors described as black, white, red, orange, yellow, blue, green, and turquoise. They have detailed hands with tapering fingers and fingernails. Toenails are also present on feet with modeled toes. Molds were used to manufacture four basic face types, allowing the production of a variety of deity images. The paste color varies from gray to cinnamon and is described as having a limestone temper. It is also mentioned that most censers have a calcareous coat, which is believed to serve as a base for applying multiple colors [9–12].

Since 1996, excavations of the last Maya capital in México, conducted by Carlos Peraza Lope from Centro INAH Yucatán, have unearthed a significantly large number of censers and sherds. Results from this project, along with documents from the Carnegie excavations in the 1950s, depict a well-established archaeological context and chronology of Mayapán's censers. Recent studies by Carlos Peraza and Marilyn Masson have also provided evidence on the spatial distribution of the censers and accounted the different types of deities represented [9–14].

In this work, we present the results of a material study of the pigments and the ceramic paste from sherds that have been archaeologically described as belonging to the ***Chen Mul*** and ***Hoal*** modeled types of effigy censers. The set of studied objects belongs to and is kept under the protection of the *Instituto Nacional de Antropología e Historia* (INAH) in Mérida, Yucatán, México. The study involves a combination of spectroscopic and imaging techniques, which share the common characteristics of being non-destructive, minimally invasive, and mobile. They allowed us to conduct the whole study in situ, where the collection is stored. Eventually, the results will allow us to establish a database and a set of techniques applicable in similar, larger, and more complex pieces, such as a complete ***Chen Mul*** effigy censer.

In our methodology, our first approach employing hyperspectral imaging (HSI) analysis provided guidelines for later applying the other complementary spectroscopic techniques. X-ray fluorescence (XRF) spectroscopy allowed us to describe the characteristic elements present in both pastes and pigment regions, while the fiber optic reflectance spectroscopy (FORS) spectral information considered the features present in the visible (such as reflectance maxima, inflection points, and absorbance maxima) and in the infrared (IR) regions.

2. Materials and Methods

2.1. Archaeological Materials

The corpus of the study comprises 63 fragments from the ***Chen Mul*** modeled censers and 9 fragments from the ***Hoal*** modeled censers found in the Mayapán region (see Figure 1). The ID codes of each piece were assigned according to the operations and excavation lots, following a control grid during the archaeological work at the Mayapán site. Since the

actual labels could be too long, or in some cases even duplicated due to the archaeological record, we decided to use condensed sequential numbers in order to facilitate the reading, keeping only the first two digits of the year of excavation. Figure 1 now exhibits those IDs, and a table is included in the Supplementary Materials. Their sizes range from about 5 cm up to 30 cm. Effigy censer fragments include anthropomorphic representations composed of hollow figures and decorations such as clothing, jewelry, fruits, and animals made by smaller fillings. Variations in the color of the pastes range from a light grey paste in most of the fragments to a reddish color in some of the objects. Most of the fragments display polychrome decorations in the form of patterns, as described in previous works [9–14], with a color palette made up of red, orange, yellow, blue, green, and black.

Figure 1. Mayapán effigy censer sherds studied in this work. A 5 cm common scale is indicated as a vertical line adjacent to the first object in the first row and adjacent to the last object in the fourth row. Photo by O. G. de Lucio and S. Ortiz.

2.2. Hyperspectral Imaging

Hyperspectral images were recorded by a Surface Optics 710VP system, with a 4.5 nm resolution and a nominal spectral range from 400 nm to 1000 nm. The image resolution for this work is 1392 × 1392 pixels. During image acquisition, two 3200 K halogen lamps continuously illuminated the object. Verification of the wavelength calibration was achieved by using a collimated argon spectral calibration lamp. By illuminating a 2-inch Spectralon certified reflectance standard (model SRT-99-050 AA-00821-000) with the halogen lamps, it was possible to describe and subtract the contributions of light source and detector efficiency. Classification, image analysis, and description of hypercubes was performed with Harris Geospatial Solutions ENVI 5.5 software. HSI generated IR pseudo-color and spectral

angle mapper (SAM) composite images. The classification workflow is described in detail in the previous works of Perez et al. [15,16]. A comprehensive explanation of the employed algorithms can be found in the work of Green [17] for the MNF process, the works of Veganzones et al. [18] and Kale et al. [19] for PPI calculation, and the work of Foglini et al. [18] for the optimization of angle thresholds. In addition to image classification, HSI provides valuable information through other means. By assigning appropriate bands to corresponding RGB channels, it is possible to produce images in infrared pseudo-color (IR-PC). This method offers direct insights about the presence of different materials on the studied objects, as certain hues are known to be associated with specific materials [15,16,20–22].

2.3. Fiber Optic Reflectance Spectroscopy (FORS)

FORS spectral measurements were recorded by using a FieldSpect-4 ASD acquisition system. The resulting spectra provide information in the visible, near infrared (NIR), and short-wave infrared (SWIR) ranges, with a 3 nm resolution for the 300–1000 nm range and 10 nm resolution for the 1000–2500 nm range. The analysis area is about 1 cm^2, and the probe was in contact with the studied object during data acquisition. The system employs a D65 standard illuminant, and the spectra acquisition time was set at 0.2 s. The system is calibrated by using an ASD Inc (Malvern Panalytical, UK). certified reflectance standard (AS-02035-000CSTM-SRM-990-362). The system also allowed us to perform colorimetry measurements by processing the spectra with the ViewSpec Pro analysis computing code. Results are expressed in the CIE Lab colorimetric system.

2.4. X-ray Fluorescence Spectroscopy (XRF)

A home-built portable X-ray system (SANDRA) was employed for describing the elemental composition of the studied fragments; this system is described in reference [23]. In brief, the system is based on a Mo X-ray source collimated to a 1 mm area and an Amptek SDD detector with the detection angle set up at 45°. Calibration of the system is achieved by using different NIST standard reference materials (Basalt rock 688, Montana 2710, Montana 2711, Bufalo 2704, 88b, 1d), thus allowing it to obtain semi-quantitative data. The acquisition parameters used were 35 kV, 0.300 mA, and a 90 s acquisition time; no filters were used during the spectra acquisition. Spectra deconvolution was performed by means of the ESRF-BLISS PyMca analysis toolkit [24].

To help discern between the elements present in the pigment and those from the ground layer, measurements were always performed on multiple areas of the substrate over which the pigment was applied.

2.5. Microscopic Analysis

Microscopic analysis was conducted using a portable USB digital microscope, specifically, the Dinolite model AF4915ZT manufactured by AnMo Electronics Corp. This microscope is equipped with integrated illumination and a polarizer for image acquisition. It offers magnification capabilities ranging from 20× to 220×, with corresponding working distances varying from 60 mm to 12 mm. The resulting images have a resolution of 1280 × 1024 pixels. Notably, the microscope system incorporates advanced image processing functionalities, including extended depth of field (EDOF) and enhanced dynamic range (EDR).

3. Results and Discussion

3.1. Global Properties of Objects

The results obtained from HSI enabled us to create pigment material mappings. These maps indicate regions with similar spectral reflectance signals, thus revealing patterns in pigment application, areas experiencing material loss, or alterations in the decoration layer. Utilizing the IR-PC images, we were able to directly identify pigments and their distribution on the objects. The results are presented as a shift in hue from the visible image (Figure 2a) to the IR image (Figure 2b). For instance, red and orange pigments transition into yellow,

indicating the use of earth materials. Similarly, blue and green pigments transform into pink, suggesting a similar nature and potentially being associated with indigo. The pastes and carbonate layer adopt an ochre hue, with varying saturation depending on the amount of carbonate present. Lighter regions correspond to areas where the carbonate layer is more pronounced. Additionally, a distinct gray zone is observed, which remains unchanged. This zone corresponds to a restoration area that can be excluded from further analysis.

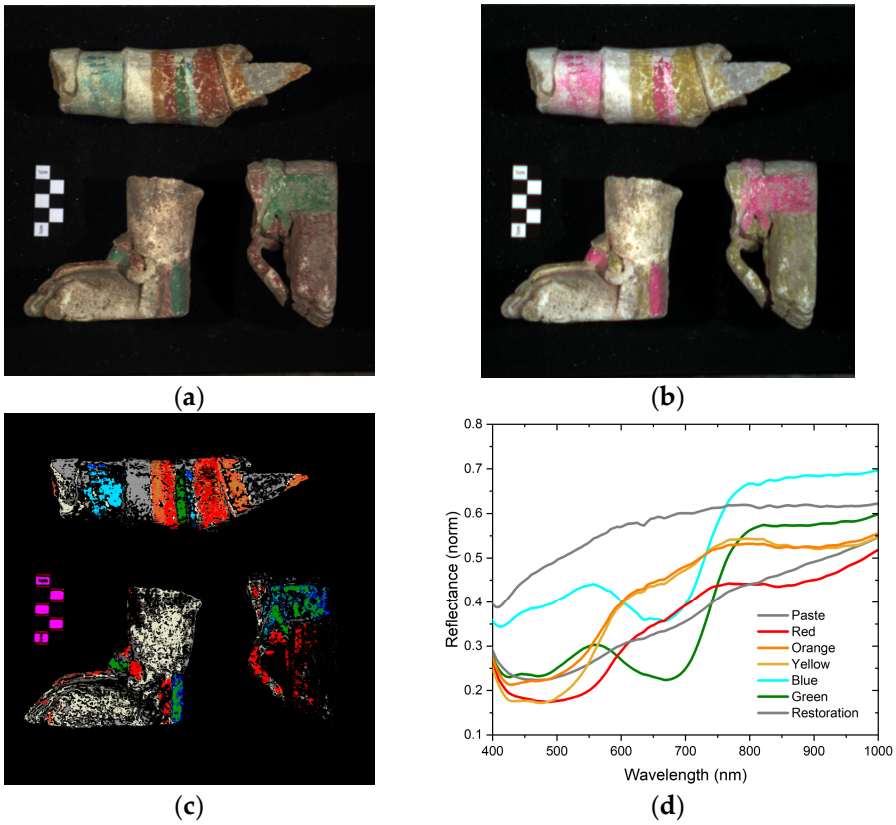

Figure 2. (**a**) RGB image of pieces 96-044 (**top**), 98-043 (**left**), and 96-009 (**right**). (**b**) IR pseudo-color image, (**c**) SAM image, where unit corresponds with 1 cm, and (**d**) endmembers representative spectra; colors correspond with SAM mapping colors.

A more detailed SAM analysis generates maps of the common materials between pieces by comparing the reflectance spectra of each pixel (as in Figure 2c). This technique also generates basic reflectance spectral information (see Figure 2d), which provides a fast and global analysis. The resulting endmember reflectance spectra from the red, orange, and yellow regions have similar iron oxide-based pigment behavior, as they have inflection points at around 550 nm and absorption bands in the 850–900 nm interval. Blue and green endmembers present a reflectance maximum near 550 nm, absorbance maximum in the 650–700 nm interval, and an abrupt reflectance increase at around 730 nm. These features confirm the similar nature of the pigments and are related to the use of indigo. The endmembers from paste zones do not have any relevant spectral features in the visible region which could be associated with a specific material. Finally, the restored gray region exhibits a different reflectance intensity and does not present any noticeable features in this spectral range.

3.2. Pastes

As described previously, most of the objects were covered with a calcareous coat, and some pieces were broken or exposed, so it was possible to distinguish between the pastes and regions in which this coat was present, but there was not any pigment. The chemical compositions of the pastes exhibit the presence of Al, Si, Ca (this last one used

for normalization), K, Fe, Ti, Mn, and Sr (Figure 3). The molecular information from FORS allowed us to establish a first approximation on the identification of the clay used during the manufacture of the censers [25]. To accomplish this, the SWIR reflectance spectra from the pastes were processed through a hull quotient correction [26] to enhance its spectral features.

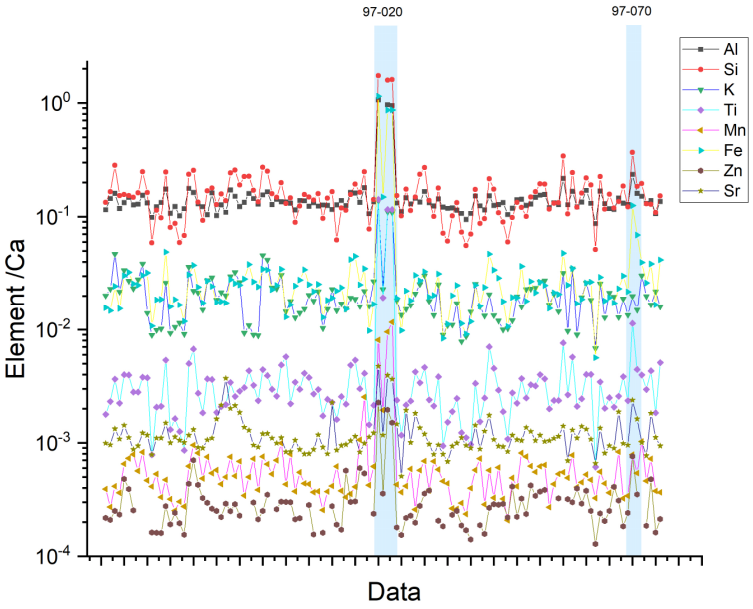

Figure 3. Principal elements in paste regions normalized with calcium. Objects with a significant deviation are marked with blue bands.

From the data, it is possible to establish an *average* elemental composition; most of the objects fall within this average and correspond with ***Chen Mul*** modeled censers from the Postclassic period (1150–1450 A.D.), which are linked to a local manufacturer as described by Peraza Lope [12]. Some objects that deviate from the *average* composition (Figure 3) can be observed, for example, results from pieces such as 97-020 (Figure 4b) that show a significantly higher concentration of elements like Si, Al, Fe, Ti, and Sr relative to Ca, while 97-070 presents a higher content of Fe and Ti. These objects are attributed to an earlier archaeological context (~1100 A.D.), and their manufacture style suggests an origin on the east coast region, as described in the works of Milbrath et al. and Peraza Lope et al. [9–14].

(**a**) (**b**)

Figure 4. A comparison between (**a**) object 96-029, whose elemental composition falls within the "average"; and (**b**) object 97-020, whose elemental composition separates noticeably.

The resulting SWIR reflectance spectra (Figure 5) of the pastes show features at around 1420 nm and 1925 nm and bands between 2200 nm–2332 nm, all of which are related with a smectite group clays. Spectral bands near 1420 nm are related to OH groups, while those around 1925 nm are related to interlaminar water in the clay structure. The interval between 2200 nm–2332 nm indicates the presence of Al-OH (2200 nm), Mg-OH (2332 nm), or Fe-OH (around 2260 nm) groups associated with laminar silicates from the smectite group, such as montmorillonite, nontronite, or saponite, as described in previous works [25–28]. It is evident that the spectrum associated with object 97-020 exhibits a distinct difference. Notably, it displays a stronger signal correlated to the Al-OH group, which aligns with the findings from XRF analysis.

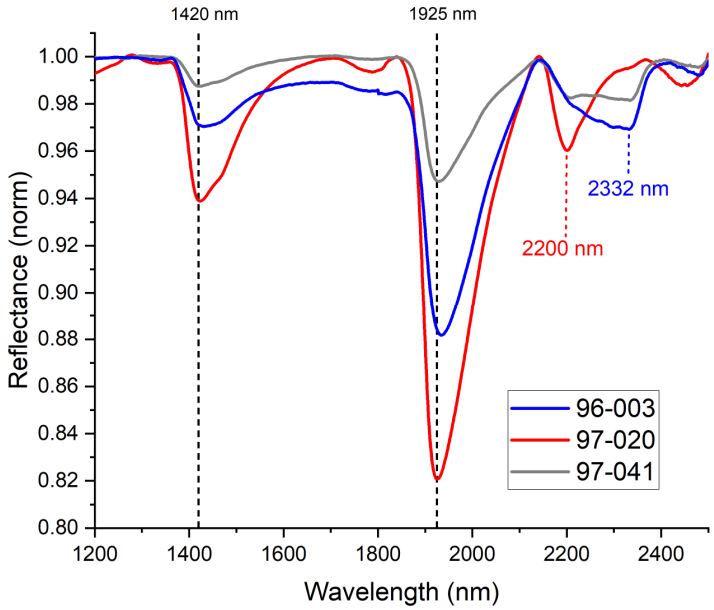

Figure 5. Example of SWIR reflectance spectra from pastes corresponding to different objects. It can be observed that object 97-020 exhibits different spectral features.

Although elemental analysis has provided evidence regarding the presence of specific materials typically associated with pastes or pigments, it is essential to note that this technique does not differentiate between information originating from the ceramic matrix, which could extend up to hundreds of microns, and the surface layer. Consequently, it is crucial to consider the insights derived from the pastes when conducting subsequent pigment analyses.

3.3. Pigments

Examples of the various colors present in the objects can be observed in detail in Figure 6. The results obtained through FORS colorimetry have proven valuable in providing a useful classification system for the subsequent application of spectroscopic techniques in specific regions of interest. This classification approach has facilitated the grouping of results based on pigment color, including black, white, red/orange, yellow, blue, and green. Furthermore, colorimetry analysis alone has revealed interesting findings regarding the distribution of green-like colors. These hues exhibited a wider dispersion across the hue coordinate, spanning approximately 60 degrees, in comparison to the other pigments, which displayed narrower distributions of 30 degrees or less (as depicted in Figure 7). This disparity may suggest that multiple techniques were employed to produce the greenish hues observed on the objects. These techniques could encompass variations in pigment mixtures, the incorporation of different raw materials, or modifications in the pigment preparation process. A summary of the main findings of the pigments analyses are presented in Table 1.

(**a**) (**b**) (**c**)

Figure 6. Examples of Mayapán's effigy censer sherds, showing the different pigments present. The unit of objects (**a**) 96-005 and (**b**) 96-034 is 1 cm; object (**c**) 96-032's unit corresponds to 0.5 cm.

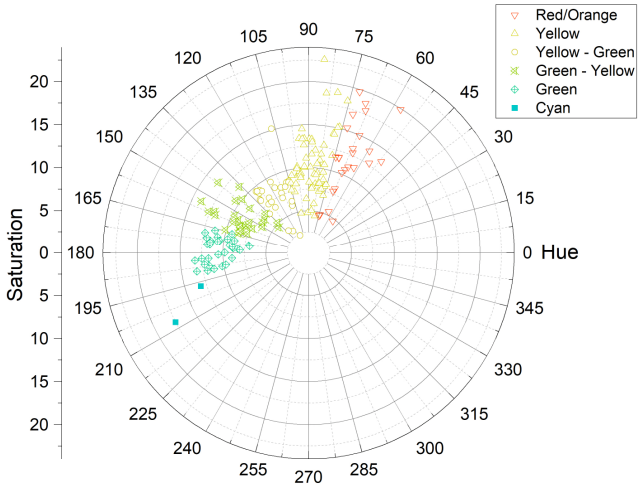

Figure 7. FORS colorimetry results for pigments (different than black or white) present on objects.

Table 1. Results from analytical techniques and principal material observed.

Related Material	Chemical Composition	XRF	FORS	HSI
Calcite	$CaCO_3$	Ca	SWIR 2337 nm	
Soil minerals		Fe, Ti, Al		
Aluminosilicate	Al_2O_5Si	Si, Al	SWIR 2200 nm–2332 nm	
Hematite	α-Fe_2O_3	Fe	Vis 850 nm	Yes
Goethite	α-FeOOH	Fe	Vis 900 nm	Yes
Maya blue		Si, Al	Vis-SWIR 2221 nm, 2253 nm	Yes
Green 1		Si, Al	Vis-SWIR 659 nm, 2253 nm	Yes
Green 2		Si, Al, Fe	Vis-SWIR 647 nm, 2253 nm	Yes

3.3.1. Black and White

An apparent black pigment, which seems to be the result of the flow of some material associated with the use of the censers [9–14], as shown in Figure 8a, presents no characteristic elements on it, and the FORS information does not exhibit any particular compound. The white pigment (Figure 8b) presents larger amounts of Ca (with less Si and Ti than the paste), and the reflectance spectra indicate that it corresponds to calcium carbonate (Figure 9) [27,28].

(**a**) (**b**)

Figure 8. (**a**) Sample of a fragment (96-061) with presence of black material. (**b**) Sample of a fragment (96-001) with white covering pigment.

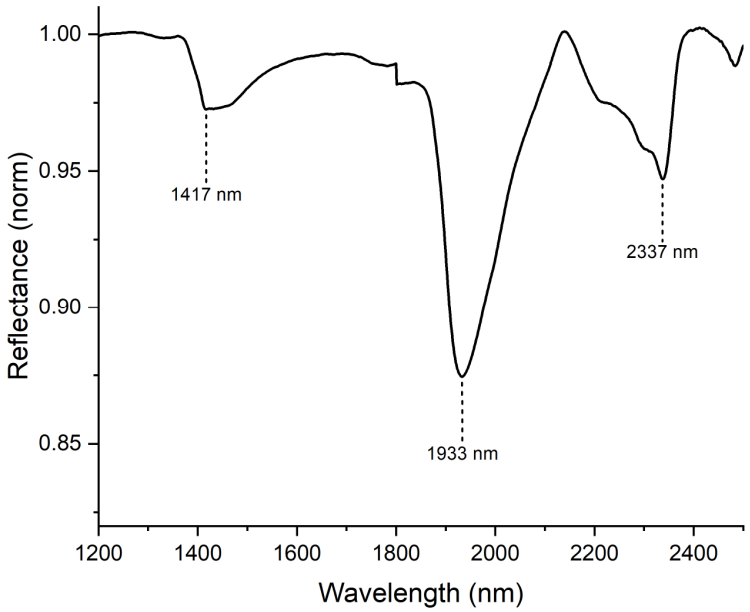

Figure 9. Spectra from a white region on object 96-001 after hull correction. It shows an absorption peak near 2337 nm associated with calcium carbonate.

3.3.2. Red, Orange, and Yellow

XRF permitted us to describe the elemental composition of red, orange, and yellow regions with major elements (Ca, Fe, Si, and Al), minor elements (Ti, K, S, and P), and trace elements in all pieces. Red, orange, and yellow regions share similar concentrations in major and minor elements (Figure 10) and show a noticeable increase in Fe and Ti with respect to the paste.

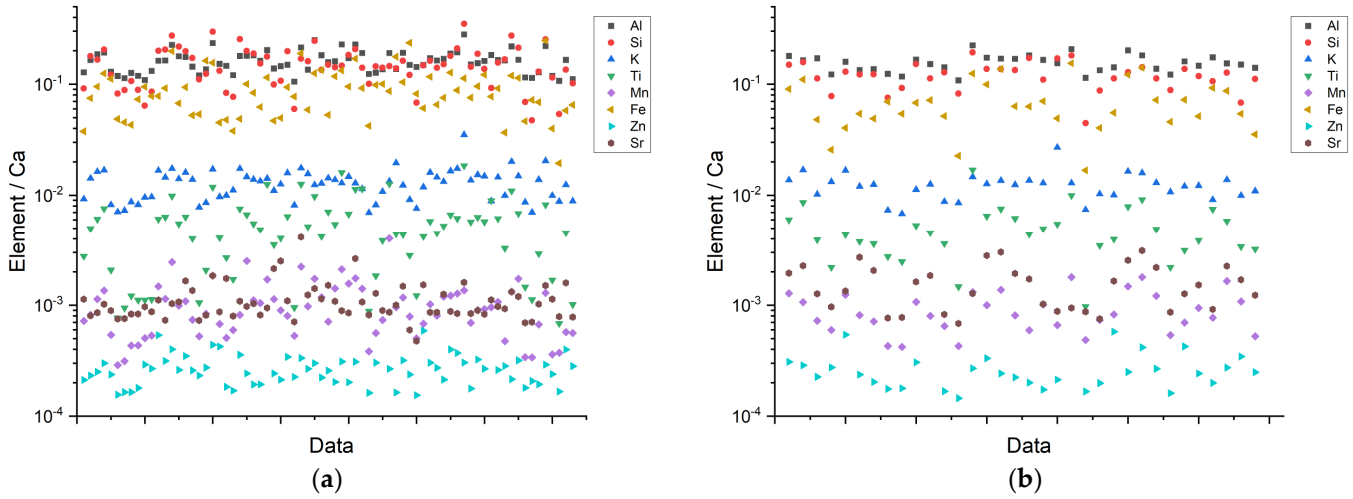

Figure 10. Characteristic elements (**a**) in red regions and (**b**) in orange/yellow regions. Data are normalized to calcium.

Iron and silicon concentrations vary in similar ranges for red and yellow zones and show a higher Fe concentration ratio than in pastes, indicating the presence of additional iron-based materials (Figure 11). If we calculate the Fe/Si ratio for red data, it is about 1.25 ± 0.44, and for yellow it is 1.6 ± 0.34, while most of the pastes show a Fe/Si ratio of about 0.18 ± 0.02, not considering the atypical objects, such as piece 97-020, which has a ratio of 0.61 ± 0.15, and piece 97-070 with a ratio of 0.29 ± 0.08.

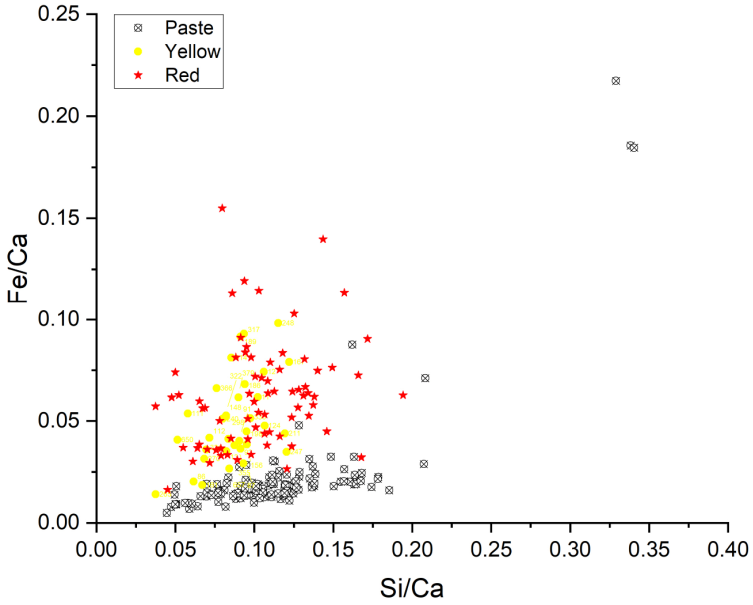

Figure 11. Elemental correlation between Fe and Si in red, yellow, and paste zones. Data are normalized to Ca.

The visible reflectance spectra from the red and yellow regions exhibit characteristic iron oxide-based pigment behavior (Figure 12). These spectra were compared with the corresponding reference spectra of goethite and hematite [28]. The comparison proved that red and orange pigments show hematite (α-Fe_2O_3)-like features, such as the inflection point and absorption maxima around 580 nm and 850 nm, respectively. Representative features from yellow pigments show goethite (α-FeOOH)-like features, such as inflection points near 550 nm and absorption maxima near 900 nm. Iron oxide absorptions in the visible region correspond to electronic transitions within the 3*d* shell [29].

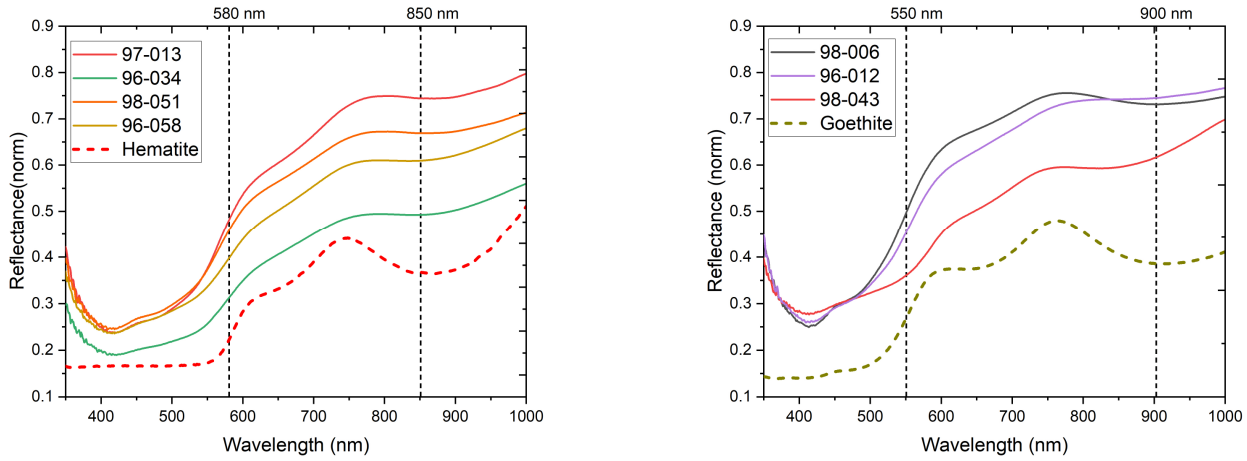

Figure 12. (**a**) Red, orange, and (**b**) yellow example reflectance spectra with principal features indicated and comparison with reference spectra for hematite and goethite according to [28].

3.3.3. Blue and Green

As mentioned before, the blue and green regions were first classified by using colorimetric data, and in the case of the green pigment, it seems likely that there could be different preparations. In order to explore this, we considered the elemental analysis results, which provide information on the major and minor elements (see Figure 13). Of particular interest is the relation between Fe and Si (Figure 14a), since it makes it possible to distinguish different data clouds and relations for the different data resulting from the paste, blue, green, and yellow areas.

It is worth noticing that in the Fe vs. Si relation, the blue and yellow data produce two different trends, with corresponding ratios of 0.067 ± 0.005 and 1.6 ± 0.34. While the green pigment exhibits two well-differentiated linear behaviors: the hue named ***green 1*** shows a slope of 0.082 ± 0.015, which is similar to that of the blue pigment within uncertainties, and the one called ***green 2*** with a slope of 0.67 ± 0.10 (Figure 14a,b).

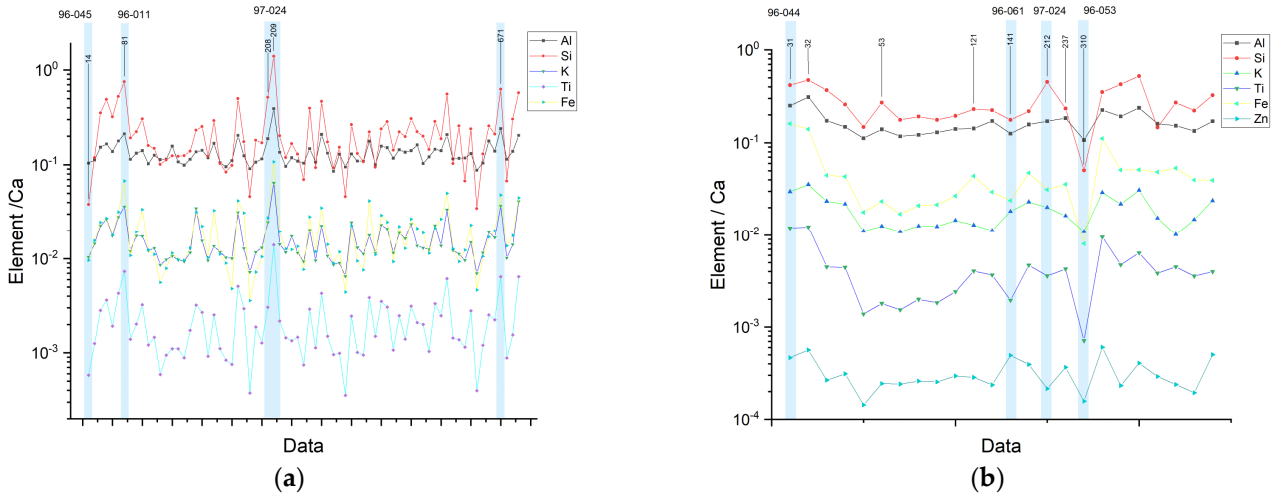

Figure 13. Principal elements from (**a**) blue regions and (**b**) green regions. Objects with a significant deviation are marked with blue bands.

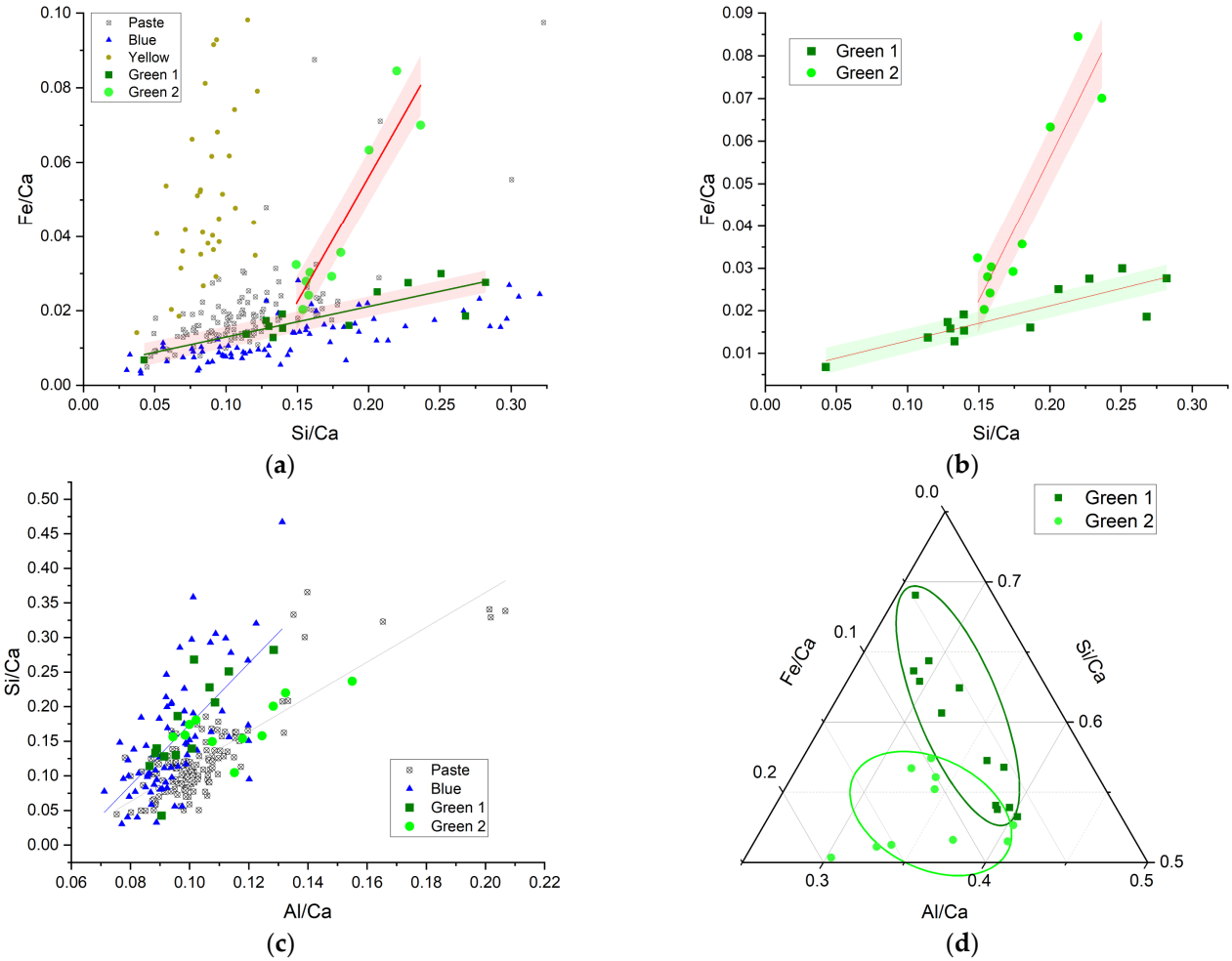

Figure 14. (**a**) Fe vs. Si data for pastes and blue, yellow, and green pigments; (**b**) Fe vs. Si data for green pigments, and in both plots, linear fits are shown with the 95% confidence band; (**c**) Si vs. Al data for pastes and blue and green pigments with the corresponding linear fits for paste and blue pigment; (**d**) ternary plot of Al, Si, and Fe for green pigments; ellipses encompassing the different groups were drawn to guide the eye.

On the other hand, relations between Si and Al for the paste, blue, and green regions were also compared (Figure 14c). Although differences between these regions are not as evident in this case as in the previous case, it is still possible to distinguish the paste with a ratio of 2.5 ± 0.2 from the blue region with a ratio of 4.4 ± 0.6. The ***green 1*** ratio (4.8 ± 1.0) is again comparable to the corresponding ratio of the blue pigment, and ***green 2*** has a slope of 1.3 ± 0.5. The information corresponding to the green pigments is also displayed as a ternary diagram for Al, Si, and Fe in Figure 14d, where it is also possible to distinguish the different trends between those two kinds of greens.

The reflectance information indicates that the blue and green regions have distinctive reflectance spectra in the SWIR region (Figure 15), with intense absorption features around 1419 nm, 1925 nm, 2221 nm, 2253 nm, and 2336 nm. As mentioned before, the feature by 1419 nm is related to vibrations from OH groups, and the one at 1925 nm is related to vibrations of groups on structural water, both associated with the paste. Bands around 2221 nm and 2253 nm are only present in blue and green regions and could be linked with a different clay present in these zones, likely palygorskite [$MgAl_2(Si_4O_{10})(OH)_2 \cdot 4H_2O$], due to the known procedures for Maya blue production [30,31].

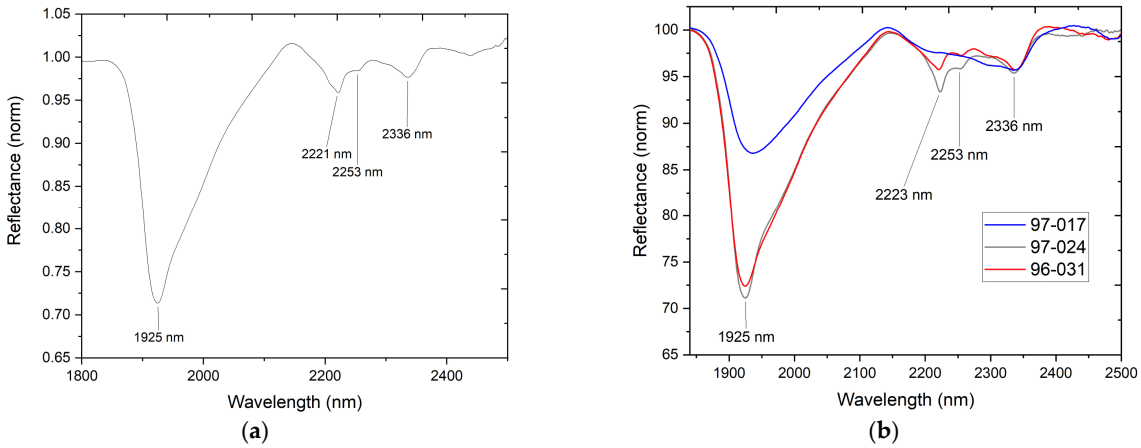

Figure 15. (**a**) Representative SWIR spectra from the blue pigment on object 96-015 and (**b**) representative objects for the green pigments. Features associated with $CaCO_3$ and clays are indicated.

As for the spectral visible region, blue pigments show a reflectance maximum near 449 nm and 530 nm and an absorbance maximum around 668 nm (Figure 16a), related to the chromophore group in the indigo molecule ($C_{16}H_{10}N_2O_2$) in Maya blue pigment [25,31]. While it has been reported that the absorption band can vary due to different synthesis procedures (different nature of clay, indigo/clay ratio, heating temperature, and time of cooking) [31], the feature near this spectral interval in Maya blue samples has been reported in previous works for samples from other regions [32].

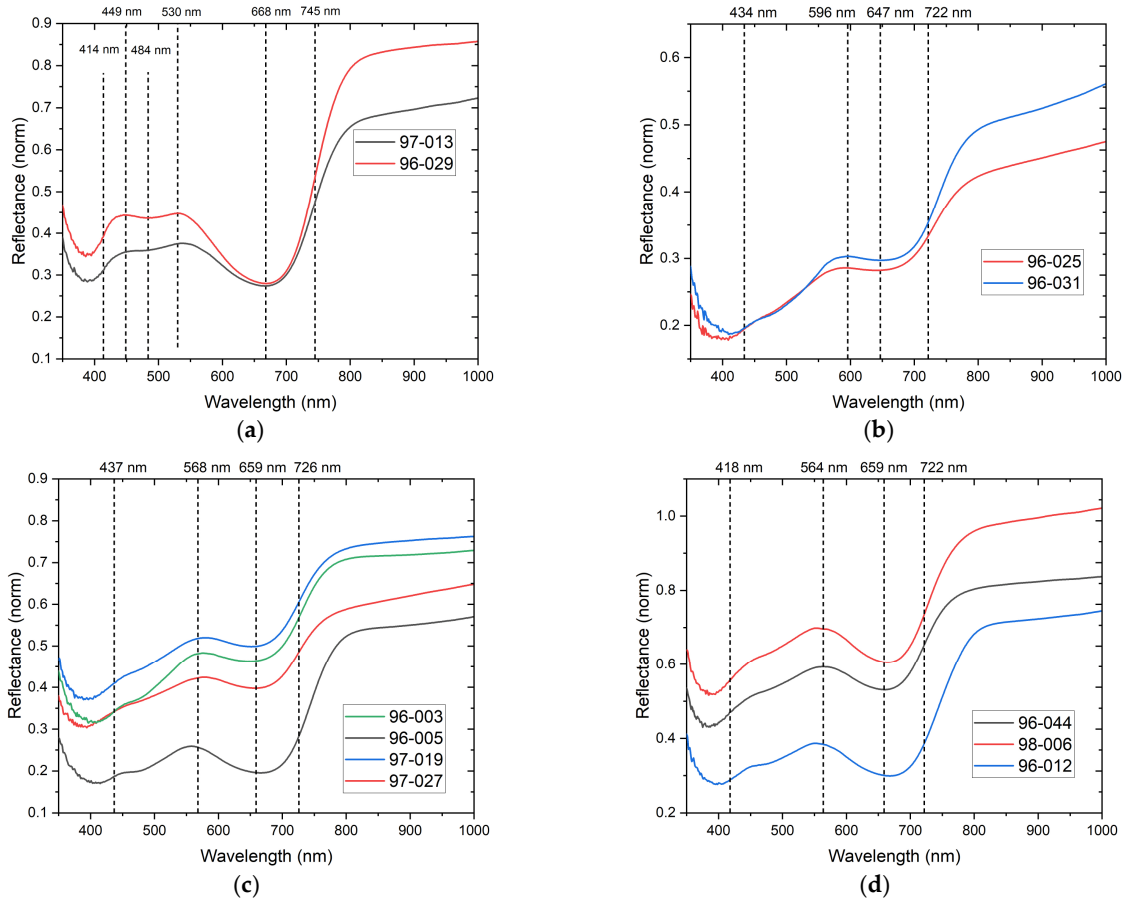

Figure 16. Representative reflectance spectra from (**a**) blue regions and (**b**–**d**) green regions.

The reflectance spectra from the green hue regions (Figure 16b–d) show inflection points between 722 nm–726 nm as a common feature. This band is close to that at the 745 nm inflection point associated with indigo. The bathochromic shift of local reflectance maxima near 596 nm in the yellowish-green group (Figure 16b) and green (Figure 16c,d) groups near 564 nm –568 nm could be associated with mixtures of blue and yellow materials [33]. To clarify this, we also present a simple calculation in Figure 17, where spectra corresponding to blue, green, and yellow pigments (all experimental results) as well as a calculated normalized spectrum resulting from the sum of a 35% yellow and 65% blue pigments are shown. As can be seen, adding these pigments results in a similar spectrum to that identified as ***green 2***.

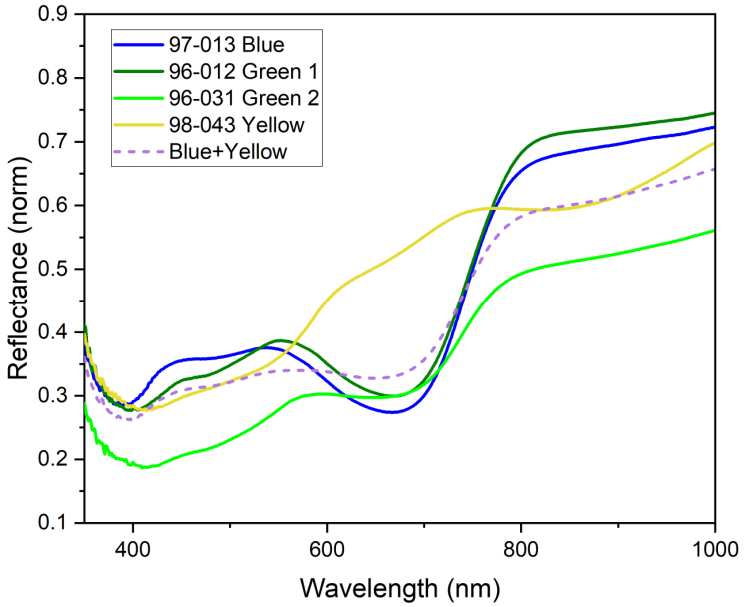

Figure 17. Comparison of experimental reflectance spectra of blue, yellow, and green regions and the sum of blue (65%) and yellow (35%) spectra.

Although a complete clay identification can be difficult by FORS alone, it provided a description of the common features between blue and green pigments with a fast, non-invasive, and portable instrument.

3.3.4. Microscopy of Green Regions

To provide additional insights into the characteristics of the two green pigments, we employed microscopy imaging as a complementary technique to reveal further distinguishing features. The acquired images were captured in situ, without physical contact. Notably, one of the primary distinguishing features observed within the green zones is the variation in both the hue and particle size of the involved pigments, as depicted in Figure 18a. In this image, a uniform color distribution is apparent, with the particles being small enough that they cannot be clearly differentiated. Conversely, in Figure 18b, other regions display the presence of relatively large blue particles, which are accompanied by a yellowish layer.

The archaeological context of the objects where the ***green 1*** and ***green 2*** pigments are observed suggests they were manufactured in the same pottery workshop. The difference in the elemental composition of the green pigments thus implies that the way of preparing the material is linked with the skills and knowledge of the craftsman. Archaeological findings suggest that the censers were produced in the same workshop; hence, we propose that the difference in chemical composition could be due to the experimentation of new materials within the workshop made by the potters who worked there. A generational change is also suggested by the style of the pieces. Previous exploration of the Q40a structure in Mayapán has allowed to establish the place of production of the ***Chen Mul*** censers. The

archaeological data also indicate a production of figurines and copper bells in the same workshop. These data suggest that the experimentation in color could have occurred in this workshop. We can also suggest that this experimentation with color is coupled with the high degree of specialization observed in the censer production workshop [9–14].

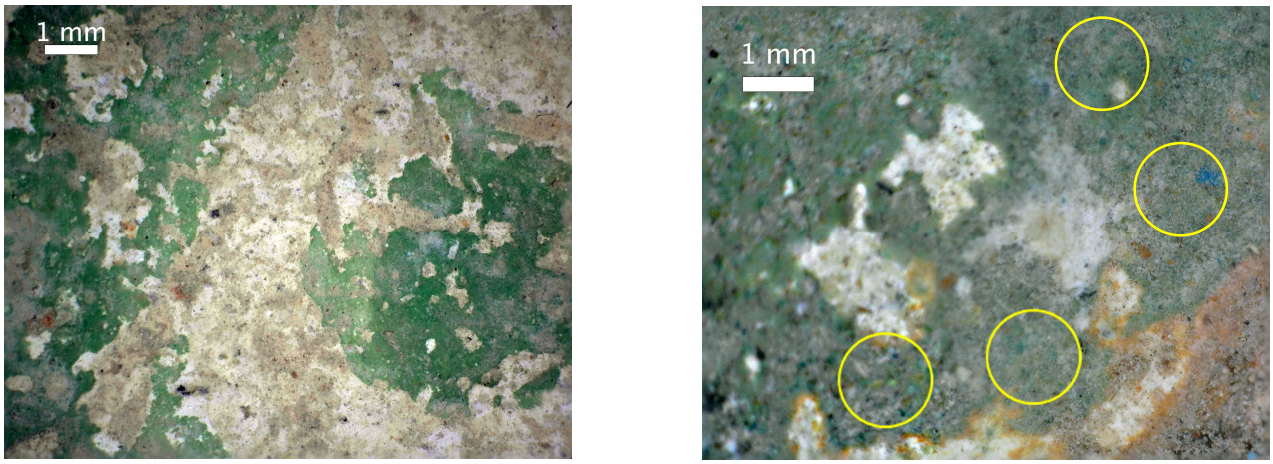

(**a**) (**b**)

Figure 18. (**a**) Uniform green layer over *stucco* at 40× corresponding to green 1, and (**b**) green region with yellow pigment layer and blue particles (position indicated with yellow circles) at 50×, corresponding to green 2.

4. Conclusions

A combination of analytical techniques permitted us to describe features from the materials in the set of samples as characteristic elements detected by XRF and absorptions in the visible, near-infrared, and mid-infrared regions. As presented in every case, the proportion of these materials vary and could be associated with differences in manufacturing, the sources of material, or the provenance of the studied objects.

Mayapán censer sherds were analyzed through a non-invasive methodology that permitted us to identify the materials and their application on the different layers that comprised them. In this methodology, information from each technique is complementary, starting with a mapping of similar materials with hyperspectral imaging, allowing us to establish if the regions of the studied objects were comparable; then, the elemental composition provides insights on the nature of the materials involved in the manufacture of the censers; and later, molecular spectroscopies provide chemical information by spectral features in the visible and NIR regions.

The palette used in the different decoration layers ranges from red, orange, and yellow pigments, which are composed primarily of iron oxide-based materials; blue, likely corresponding to the well-known Maya blue; and green, which we were able to identify two different preparations of, one directly related and very similar with that of Maya blue, and the other which could be a mix of different materials or a significant variation on the proportion of the clay.

As for the pastes, by using SWIR analysis, it was possible to characterize calcium carbonate and provide insights on the presence of smectite-group clays with a variable proportion of Al–OH, Mg–OH, and Fe–OH groups. This variation was also detected in XRF analysis through samples and could be related with the specific clay fraction.

No significant material differences between the ***Chen Mul*** and ***Hoal*** modeled censer types were detected, except for the pieces 97-070 and 97-020, which are likely to be imports from the east coast region.

Although non-invasive elemental techniques provide adequate results, they are limited when a description of composite or multilayered materials is required since several physical parameters must be taken into account, thus requiring more complex analytical models. In

our investigation, reflectance spectroscopy provided a fast tool for determining at a first approximation the clays employed in the manufacture of the ceramic objects, but such characterization still requires confirmation by drawing micro-destructive techniques such as XRD or thin-section petrographic analysis.

Supplementary Materials: The following supporting information can be downloaded at: https://www.mdpi.com/article/10.3390/min13070974/s1, Table S1: List of studied objects, with associated identifier code and related XRF and FORS spectra.

Author Contributions: M.P.: Writing—original draft, Methodology, Software, Formal analysis, Investigation. O.G.d.L.: Writing—review and editing, Methodology, Visualization, Investigation, Funding acquisition, Project administration. A.M.: Writing—review and editing, Formal analysis, Investigation. C.P.L.: Archaeological Research Manager, Writing—review, Archaeological Investigation. W.C.A.: Writing—review, Archaeological Investigation. S.O.R.: Writing—review and editing, Methodology, Archaeological Investigation, Archaeological Findings Interpretation. All authors have read and agreed to the published version of the manuscript.

Funding: This research work was supported by project **CONACYT CF 2019 No. 731762**; and by CONACYT grants LN293904, LN 299076, LN314846, LN315853 and by DGAPA-PAPIIT grants IN101920, IN113321 and IN108521. Miguel Pérez and Soledad Ortiz acknowledge their postdoctoral fellowship granted by CONACYT.

Data Availability Statement: Spectral databases will be available on request.

Acknowledgments: Experimental results were possible due to the support granted by *Laboratorio Nacional de Ciencias para la Investigación y Conservación del Patrimonio Cultural* (LANCIC-IF).

Conflicts of Interest: The authors declare no conflict of interest.

References

1. Pollock, H.E.D. Introduction. In *Mayapan, Yucatan, Mexico*; Pollock, H.E.D., Roys, R.L., Proskouriakoff, T., Ledyard, A., Eds.; Carnegie Institution of Washington: Washington, DC, USA, 1962; pp. 1–25.
2. Smith, A.L. Residential and Associated Structures at Mayapan. In *Mayapan, Yucatan, Mexico*; Pollock, H.E.D., Roys, R.L., Proskouriakoff, T., Ledyard, A., Eds.; Carnegie Institution of Washington: Washington, DC, USA, 1962; pp. 165–320.
3. Russell, B.W. Postclassic Maya Settlement on the Rural-Urban Fringe of Mayapán, Yucatán, Mexico. Doctoral Dissertation, Department of Anthropology, University at Albany, New York, NY, USA, 2008.
4. Haviland, W.A. The Book of Chilam Balam of Chumayel. *Am. J. Phys. Anthropol.* **1967**, *27*, 402–403. [CrossRef]
5. Edmonson, M.S. The Ancient Future of the Itza. In *The Book of Chilam Balam of Tizimin*; University of Texas Press: Austin, TX, USA, 1982.
6. Alcalá, E.S. *Códice Pérez: Traducción Libre Del Maya al Castellano*; Edición de la Liga de Acción Social: Mérida Yucatán, México, 1949.
7. De Landa, D. *Relación de Las Cosas de Yucatán*, 8th ed.; Editorial Porrúa, S. A.: México City, México, 1986.
8. Smith, R.E. *The Pottery of Mayapan Including Studies of Ceramic Material from Uxmal, Kabah, and Chichen Itza*; Peabody Museum of Archaeology and Ethnology, Harvard University: Cambridge, MA, USA, 1971.
9. Milbrath, S.; Lope, C.P. Mayapán's Chen Mul Modeled Effigy Censers. In *Ancient Maya Pottery*; University Press of Florida: Gainesville, FL, USA, 2013; pp. 203–225.
10. Milbrath, S.; Aimer, J.; Peraza Lope, C.; Florey-Folan, L. Effigy Censers of the Chen Mul Modeled Ceramic System and Their Implications for Late Postclassic Maya Interregional Interaction. *Mexicon* **2008**, *30*, 104–112.
11. Milbrath, S. Los Incensarios Efigie de Mayapán: Iconografía, Contexto y Conexiones Externas. *Famsi* **2007**, *2*, 21–34.
12. Peraza Lope, C.; Masson, M.A.; Cruz Alvarado, W.; Russell, B.W. Effigy Censer and Figurine Production at the Postclassic Maya City of Mayapan, Mexico. *Anc. Mesoam.* **2023**, *34*, 455–475. [CrossRef]
13. Masson, M.A.; Peraza Lope, C. *Kukulcan's Realm*; Universty Press of Colorado: Boulder, CO, USA, 2014.
14. Peraza Lope, C.; Masson, M.A.; Hare, T.S.; Cruz Alvarado, W.; Flores Coba, L. Pottery Assemblage Variation at Mayapán Residences. In *Settlement, Economy and Society at Mayapan, Yucatan, Mexico*; Masson, M.A., Hare, T.S., Peraza Lope, C., Rusell, B.W., Eds.; University of Pittsburg Center for Comparative Archaeology: Pittsburg, PA, USA, 2021; pp. 223–254.
15. Pérez, M.; Arroyo-Lemus, E.; Ruvalcaba-Sil, J.L.; Mitrani, A.; Maynez-Rojas, M.A.; de Lucio, O.G. Technical Non-Invasive Study of the Novo-Hispanic Painting the Pentecost by Baltasar de Echave Orio by Spectroscopic Techniques and Hyperspectral Imaging: In Quest for the Painter's Hand. *Spectrochim. Acta A Mol. Biomol. Spectrosc.* **2021**, *250*, 119225. [CrossRef] [PubMed]
16. Pérez, M.; Cano, N.; Ruvalcaba-Sil, J.L.; Mitrani, A.; de Lucio, O.G. Technical Non-Invasive Study of an 18th Century Novo-Hispanic Panel Painting. *Heritage* **2021**, *4*, 3676–3696. [CrossRef]
17. Green, A.A.; Berman, M.; Switzer, P.; Craig, M.D. A Transformation for Ordering Multispectral Data in Terms of Image Quality with Implications for Noise Removal. *IEEE Trans. Geosci. Remote Sens.* **1988**, *26*, 65–74. [CrossRef]

18. Veganzones, M.A.; Graña, M. Endmember Extraction Methods: A Short Review. In *Knowledge-Based Intelligent Information and Engineering Systems*; Springer: Berlin/Heidelberg, Germany, 2008; pp. 400–407. [CrossRef]
19. Kale, K.V.; Solankar, M.M.; Nalawade, D.B. Hyperspectral Endmember Extraction Techniques. In *Processing and Analysis of Hyperspectral Data*; IntechOpen: London, UK, 2020; Volume I, p. 13.
20. Foglini, F.; Grande, V.; Marchese, F.; Bracchi, V.A.; Prampolini, M.; Angeletti, L.; Castellan, G.; Chimienti, G.; Hansen, I.M.; Gudmundsen, M.; et al. Application of Hyperspectral Imaging to Underwater Habitat Mapping, Southern Adriatic Sea. *Sensors* **2019**, *19*, 2261. [CrossRef] [PubMed]
21. Fang, Q.; Hong, H.; Zhao, L.; Kukolich, S.; Yin, K.; Wang, C. Visible and Near-Infrared Reflectance Spectroscopy for Investigating Soil Mineralogy: A Review. *J. Spectrosc.* **2018**, *2018*, 3168974. [CrossRef]
22. Hayem-Ghez, A.; Ravaud, E.; Boust, C.; Bastian, G.; Menu, M.; Brodie-Linder, N. Characterizing Pigments with Hyperspectral Imaging Variable False-Color Composites. *Appl. Phys. A Mater. Sci. Process.* **2015**, *121*, 939–947. [CrossRef]
23. Ruvalcaba Sil, J.L.; Ramírez Miranda, D.; Aguilar Melo, V.; Picazo, F. SANDRA: A Portable XRF System for the Study of Mexican Cultural Heritage. *X-ray Spectrom.* **2010**, *39*, 338–345. [CrossRef]
24. Solé, V.A.; Papillon, E.; Cotte, M.; Walter, P.; Susini, J. A Multiplatform Code for the Analysis of Energy-Dispersive X-Ray Fluorescence Spectra. *Spectrochim. Acta Part B At. Spectrosc.* **2007**, *62*, 63–68. [CrossRef]
25. Báscones, A.; Suárez, M.; Ferrer-Julià, M.; García-Meléndez, E.; Colmenero-Hidalgo, E.; Quirós, A. Characterization of Clay Minerals and Fe Oxides through Diffuse Reflectance Spectroscopy (VNIR-SWIR). *Rev. Teledetección* **2020**, *2020*, 49. [CrossRef]
26. Bishop, J.L. Visible and Near-Infrared Reflectance Spectroscopy Laboratory Spectra of Geologic Materials. In *Remote Compositional Analysis: Techniques for Understanding Spectroscopy, Mineralogy, and Geochemistry of Planetary Surfaces*; Bishop, J.L., Bell, J.F., III, Moersch, J.E., Eds.; Cambridge University Press: Cambridge, UK, 2019; pp. 68–101, ISBN 9781316888872.
27. ASD Inc. *TerraSpec Starter Pack: Practical Applications Guide to Using the TerraSpec in Exploration and Mining*; AusSpec International Ltd.: Queenstown, New Zealand, 2012.
28. Mason, G.T.; Amdt, R.E. *Mineral Resources Data System (MRDS): USGS Data Series 20*; United States Geological Survey: Reston, VA, USA, 1996. [CrossRef]
29. Torrent, J.; Barrón, V. Diffuse Reflectance Spectroscopy of Iron Oxides. In *Encyclopedia of Surface and Colloid Science*; Taylor & Francis Group: Abingdon, UK, 2002; Volume 1, pp. 1438–1446.
30. Leona, M.; Casadio, F.; Bacci, M.; Picollo, M. Identification of the Pre-Columbian Pigment Maya Blue on Works of Art by Noninvasive UV-Vis and Raman Spectroscopic Techniques. *J. Am. Inst. Conserv.* **2004**, *43*, 39–54. [CrossRef]
31. Grazia, C.; Buti, D.; Amat, A.; Rosi, F.; Romani, A.; Domenici, D.; Sgamellotti, A.; Miliani, C. Shades of Blue: Non-Invasive Spectroscopic Investigations of Maya Blue Pigments. From Laboratory Mock-Ups to Mesoamerican Codices. *Herit. Sci.* **2020**, *8*, 1–20. [CrossRef]
32. Dejoie, C.; Dooryhee, E.; Martinetto, P.; Blanc, S.; Bordat, P.; Brown, R.; Porcher, F.; Del Rio, M.S.; Strobel, P.; Anne, M.; et al. Revisiting Maya Blue and Designing Hybrid Pigments by Archaeomimetism. *arXiv* **2010**, arXiv:1007.0818. [CrossRef]
33. Aceto, M.; Agostino, A.; Fenoglio, G.; Idone, A.; Gulmini, M.; Picollo, M.; Ricciardi, P.; Delaney, J.K. Characterisation of Colourants on Illuminated Manuscripts by Portable Fibre Optic UV-Visible-NIR Reflectance Spectrophotometry. *Anal. Methods* **2014**, *6*, 1488–1500. [CrossRef]